Front. Earth Sci. 2023, 17(1): 310–321
https://doi.org/10.1007/s11707-022-1001-6

RESEARCH ARTICLE

Organic matter pore characteristics of over-mature marine black shale: a comparison of organic fractions with different densities

Shitan NING[1], Peng XIA (✉)[1,2,3], Niuniu ZOU[1,2], Yi ZHONG[1], Yin YU[1], Yuliang MOU[1,2], Ke WANG[1,2]

1 College of Resources and Environmental Engineering, Guizhou University, Guiyang 500025, China
2 Key Laboratory of Karst Georesources and Environment Ministry of Education, Guizhou University, Guiyang 500025, China
3 School of Geosciences, China University of Petroleum, Qingdao 266580, China

© Higher Education Press 2022

Abstract Organic matter pores are considered to be the most important type of pore for preserving hydrocarbon gases in shale gas reservoirs. The organic matter in each over-mature marine shale sample was separated into two organic fractions with densities of greater than and less than 1.25 g/cm^3, and then their molecular compositions and pore characteristics were quantitatively evaluated using solid state ^{13}C-nuclear magnetic resonance (NMR) and gas (N_2 and CO_2) adsorption analyses, respectively. The results revealed that aromatic carbon is the dominant molecular composition of the over-mature organic matter in the Lower Cambrian Niutitang shale. During the over-mature stage, the organic fractions with densities of greater than and less than 1.25 g/cm^3 have no significant differences in molecular composition. The organic fractions with densities of greater than and less than 1.25 g/cm^3 do have significant differences in their organic pore characteristics. In contrast to the high density organic fraction, the low density fraction contained abundant micropores and lacked mesopores and macropores. The organic pore structures of the different occurrence states of organic matter were significantly different. The C/O of organic matter in different occurrence states are obviously different, which proves that the organic pore structure is closely related to both the occurrence state and density of the organic matter. However, these relationships are still unclear and require further study.

Keywords pore characteristics, organic matter, black shale, Early Cambrian, Yangtze Block

1 Introduction

As an unconventional natural gas reservoir, shale has an ultrafine pore size and low porosity and permeability compared with conventional sandstone reservoirs (Clarkson et al., 2012; Milliken et al., 2013; Hu et al., 2018; Feng et al., 2020; Zhang et al., 2020; Wang et al., 2022a). The ultrafine pore size of shale is not only determined by its fine grain size but also greatly affected by the organic matter it contains. Previous studies have demonstrated that the organic matter makes the largest contribution to the porosity (> 60%) of shale reservoirs, especially for organic-rich shale reservoirs, while the contributions of the minerals are usually small (Slatt and O'Brien, 2011; Milliken et al., 2013; Ji et al., 2019; Dong et al., 2021; Wang et al., 2021; Xia et al., 2021).

In addition to the thermal maturity, the type of organic matter is a significant controlling factor in the development of organic matter pores in shale. In general, pores are more developed in types I and II kerogen than in type III kerogen owing to the high hydrocarbon generation potentials of types I and II (Loucks et al., 2012; Liu et al., 2022). Using scanning electron microscopy and reflected-light microscopy, Liu et al. (2022) determined that secondary pores develop in the solid bitumin or pyrobitumin after hydrocarbon expulsion, while terrigenous organic matter, including vitrinite and inertinite, can host primary cellular pores but lack secondary pores. It is noteworthy that over-mature marine shale usually only contains type I kerogen, and its macerals are difficult to identify based on the fluorescence properties. For this type of shale, using scanning electron microscopy, Hong et al. (2020) qualitatively determined that migrated bitumen is much more porous than primary kerogen, and organic matter pores with circular or irregular shapes are well developed in bitumen but are rare in spherical organic matter and graptolites. However, the quantitative characteristics and differences in the pores in the different organic fractions in over-mature shale are still unknown. The main difficulty is the separation of the organic

Received October 29, 2021; accepted June 13, 2022

E-mail: pxia@gzu.edu.cn

fractions in this type of shale because the fluorescence extractability and the solubility of the organic matter are weak during the over-mature stage.

Density is a significant physical property of organic matter, and it has been successfully used to separate the macerals in coal (Dyrkacz et al., 1984; Guo et al., 2013; Yan et al., 2019). However, the separation of the organic fractions in over-mature marine shale using density has been poorly studied. Pyrobitumen and kerogen residue are the main organic matter fractions in over-mature marine shale and belong to sapropelite. The density of the sapropel group is less than 1.25 g/cm^3. However, some organic matter fractions are mixed and symbiotic with other minerals (such as organic clay complex, mutually wrapped organic matter, etc.) in shale, which leads to the density of organic matter fractions in this part being much higher than that of sapropelite (Xu et al., 2018; Zhang et al., 2019). It should be noted that the density of 1.25 g/cm^3 was selected because the average density of the organic matter in the Niutitang black shale is about 1.25 g/cm^3. Thus, the organic matter in the shale samples was separated using this density threshold to obtain the light and heavy fractions of the organic matter. Using scanning electron microscopy, recent studies have determined that the pore structures of pyrobitumen and kerogen residue are significantly different (Hong et al., 2020; Wang et al., 2020; Xie et al., 2021), but the quantitative pores characteristics of these fractions are still unknown.

In this study, two typical black shale samples from the Lower Cambrian Niutitang Formation were selected. The organic matter fractions in these samples were separated using a density threshold of 1.25 g/cm^3. The molecular compositions and pore characteristics were quantitatively evaluated using solid state ^{13}C-nuclear magnetic resonance (NMR) and gas (N_2 and CO_2) adsorption analysis, respectively. The goal of this study was to explore the relationships between the pore characteristics, occurrence states, and density of the organic matter in over-mature marine shale.

2 Materials and methods

2.1 Sample collection and preparation

Two fresh black shale samples were collected from the GZW section in north western Guizhou Province and the XZL section in northern Guizhou Province (Fig. 1(a)). In both sections, the sampling location was near the Ni-Mo polymetallic layer, and the representative stratigraphic columns are shown in Fig. 1(b). The mineral compositions, total organic carbon (TOC) content, and

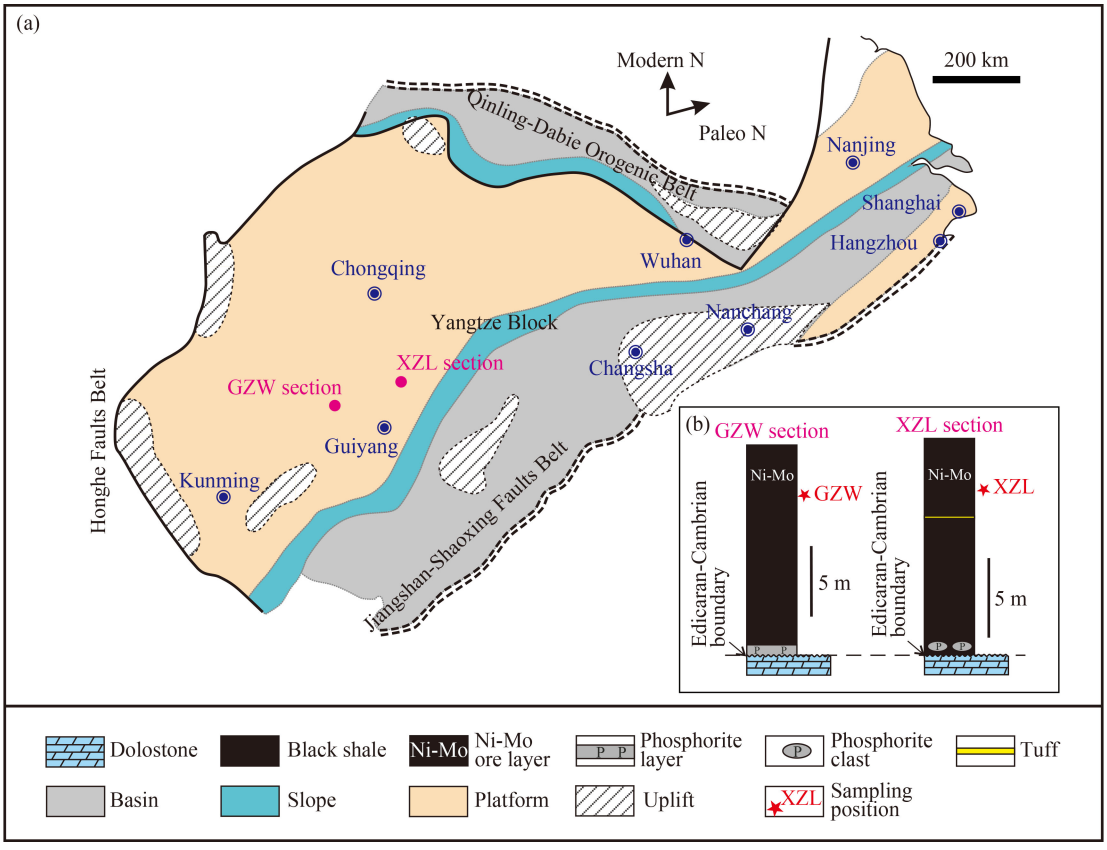

Fig. 1 Paleoenvironmental reconstruction of the Yangtze Block during the Ediacaran-Cambrian transition: (a) Paleogeographic map of Yangtze Block; (b) sampling locations (modified from Chen et al., 2009; Ning et al., 2021).

equivalent vitrinite reflectance (R_o) of these shales were measured at the China University of Petroleum, and the results are presented in Table 1. The qualitative characteristics of their minerals, organic matter, and pores were observed using a scanning electron microscope, and several images are presented in Figs. 6 and 7.

2.2 Kerogen separation

We select black shale samples with high TOC for kerogen separation, and first the shale samples were crushed into powder with size of 200 mesh using a ball milling instrument. The kerogen in these shale samples were isolated following the Chinese national standard "Isolation method for kerogen from sedimentary rock (GB/T 19144–2010 (2010))". About 10 g of kerogen were purified using chloroform for 72 h, and the kerogen was wrapped in tinfoil after being naturally dried in a fume hood. The detailed procedure of kerogen isolation is shown in Fig. 2.

Flotation liquid with a density of 1.25 g/cm^3 was prepared using the following method. 1) Iron metatungstate (i.e., the heavy liquid) was poured into a beaker, and 2) a mixture of ethyl alcohol and water with a volume ratio of 1:2 was added to the beaker to dilute the heavy liquid until its density was 1.25 g/cm^3.

The kerogen powders and flotation liquid were mixed in a centrifuge tube with a volume ratio of 1:20, and then the mixture was centrifuged at 5000 r/min for 30 min. After this, the sample was let stand for 10 min, and the supernatant was filtered through a 0.22-μm nylon membrane to retrieve the kerogen fraction with a density of less than 1.25 g/cm^3 (labeled as GZW-1 and XZL-1). The remainder of the sample was washed using distilled water and was filtered through a 0.22 μm nylon membrane to retrieve the kerogen fraction with a density of greater than 1.25 g/cm^3 (labeled as GZW-2 and XZL-2).

Table 1 Minerals compositions, TOC content, and equivalent vitrinite reflectance (Ro) of studied shales

Sample ID	Minerals compositions/%							TOC content/ %	R_o/%
	Quartz	Plagioclase	Dolomite	Siderite	Pyrite	Barite	Clay		
XZL	19.6	7.2	8.5	4	0.8	0	59.2	6.6	2.7
GZW	58.6	5.7	2.3	1.5	3.6	6.3	21.3	8.78	2.5

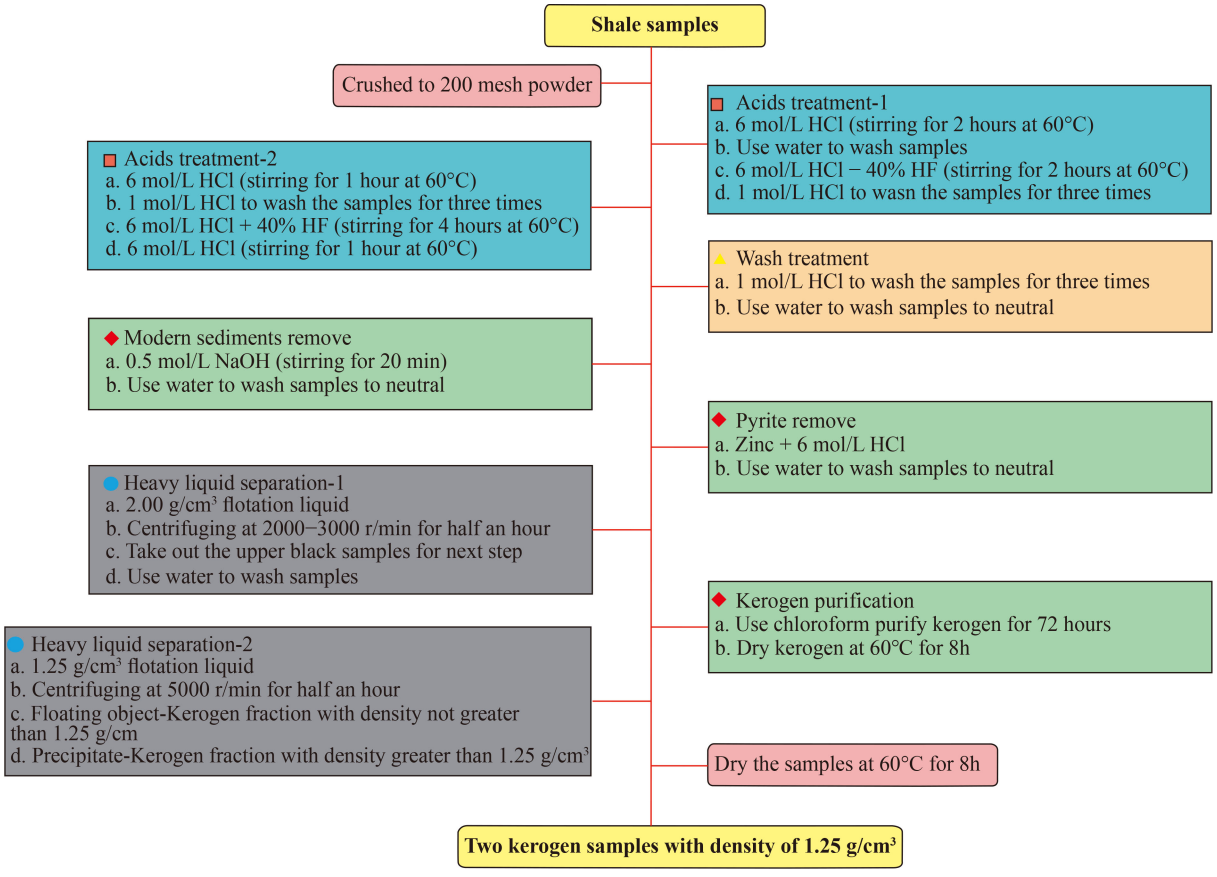

Fig. 2 A flow diagram of kerogen isolation (according to "Isolation method for kerogen from sedimentary rock" (GB/T 19144-2010)).

2.3 Experimental methods

The kerogen fractions (GZW-1, XZL-1, GZW-2, and XZL-2) were subsequently subjected to solid-state ^{13}C-NMR analysis at the Hefei Institutes of Physical Science, Chinese Academy of Sciences, and low-pressure gas (including N_2 and CO_2) adsorption measurements at the China University of Petroleum.

^{13}C-NMR analysis technology is widely used in organic chemical analysis. It is an effective method to analyze the structure of organic molecules. With the development of ^{13}C-NMR techniques such as high-power decoupling, cross-polarization, magic angle rotation and sideband suppression, the application of ^{13}C-NMR spectrum in kerogen structure analysis is increasing (Gao et al., 2017; Liu et al., 2021; Wang et al., 2022b). Its advantages are mainly that the samples are not destroyed in the analysis and it can be used for purposes after the experiment. The chemical shift is wider, and the resolution is higher than that of hydrogen spectrum. Quantitative information on a variety of functional groups can be obtained. The solid-state ^{13}C-NMR experiments were performed using a Bruker AVANCE III 600 spectrometer with a resonance frequency of 119.20 MHz. ^{13}C magic-angle spinning (MAS) NMR spectra with high-power proton decoupling were recorded using a 4-mm probe with a spinning rate of 12 kHz, a π/2 pulse length of 3.60 μs, a 1H decoupling strength of 80 kHz, and a recycle delay of 2.0 s. The chemical shifts of the ^{13}C were externally referenced to tetramethyl silane (TMS).The low-pressure gas (N_2 and CO_2) adsorption measurements were conducted using an ASAP 2460 automatic specific surface area and pore size apparatus. N_2 adsorption can be used to characterize the 1.70 to 300 nm pores (Chen et al., 2017), mainly including mesopores and macropores, whereas CO_2 adsorption is an effective method of micropore characterization (Okolo et al., 2015). Based on the gas adsorption measurements, the Brunauer-Emmett-Teller (BET) theory (Wang et al., 2015) was used to calculate the total specific surface area. The micropore volume and the micropore specific surface area were calculated using density function theory (DFT) (Klimakow et al., 2012; Han et al., 2016), and the meso-macropore volume and meso-macropore specific surface area were calculated using the Barrett-Joyner-Halenda (BJH) theory (Joyner et al., 1951).

3 Results and discussion

3.1 Compositions and lithofacies

According to the lithofacies division scheme of Ning et al. (2021), the mineral compositions of platform, slope and basin were collected for lithofacies analysis (Fig. 3). As shown in Fig. 3, argillaceous shale and siliceous shale are predominant in the inner shelf. A portion of siliceous shale and a small amount of mixed shale with carbonate shale belong to the slope region. Siliceous shale is predominant in the deep basin Clay minerals and quartz have a strong relationship with organic matter (Xia et al., 2020; Yuan et al., 2021). Considering these, the most representative siliceous and argillaceous shale from the inner shelf were selected in this study. The mineral compositions and TOC contents of the two shale samples are presented in Table 1. Both samples are organic-rich shales with TOC contents of 8.78% (sample GZW) and 6.60% (sample XZL), and they are in the over-mature stage of thermal evolution. Shale sample GZW is rich in quartz, and shale sample XZL is rich in clay mineral. As a result, the GZW shale is siliceous shale, and sample XZL is argillaceous shale.

3.2 Structural characteristics of different organic fractions

The ^{13}C-NMR spectra were fitted with Gaussian curves using the Origin 7.5 software. Figure 4(a) shows the raw curves and the compositions of the different types of carbon in the different organic fractions of shale sample XZL. In both the XZL-1 and XZL-2 fractions, the aromatic carbon region contains a peak, while both the aliphatic carbon and carbonyl carbon regions are flat (Fig. 4(a)), indicating that aromatic carbon is the dominant type of carbon in both fractions.

As is shown in Fig. 4(b), XZL-1 contains a large proportion of protonated aromatic carbon (96.82%), and the remaining 3.18% is bridgehead aromatic carbon. In contrast to XZL-1, the protonated aromatic carbon content of XZL-2 is higher (99.22%), and it contains 0.59% bridgehead aromatic carbon and 0.19% oxygen

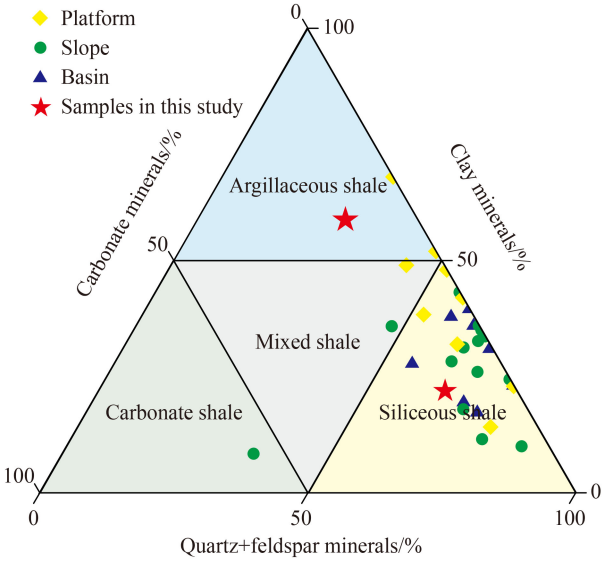

Fig. 3 Lithofacies division scheme of GZW and XZL of marine shale (modified from Ning et al., 2021).

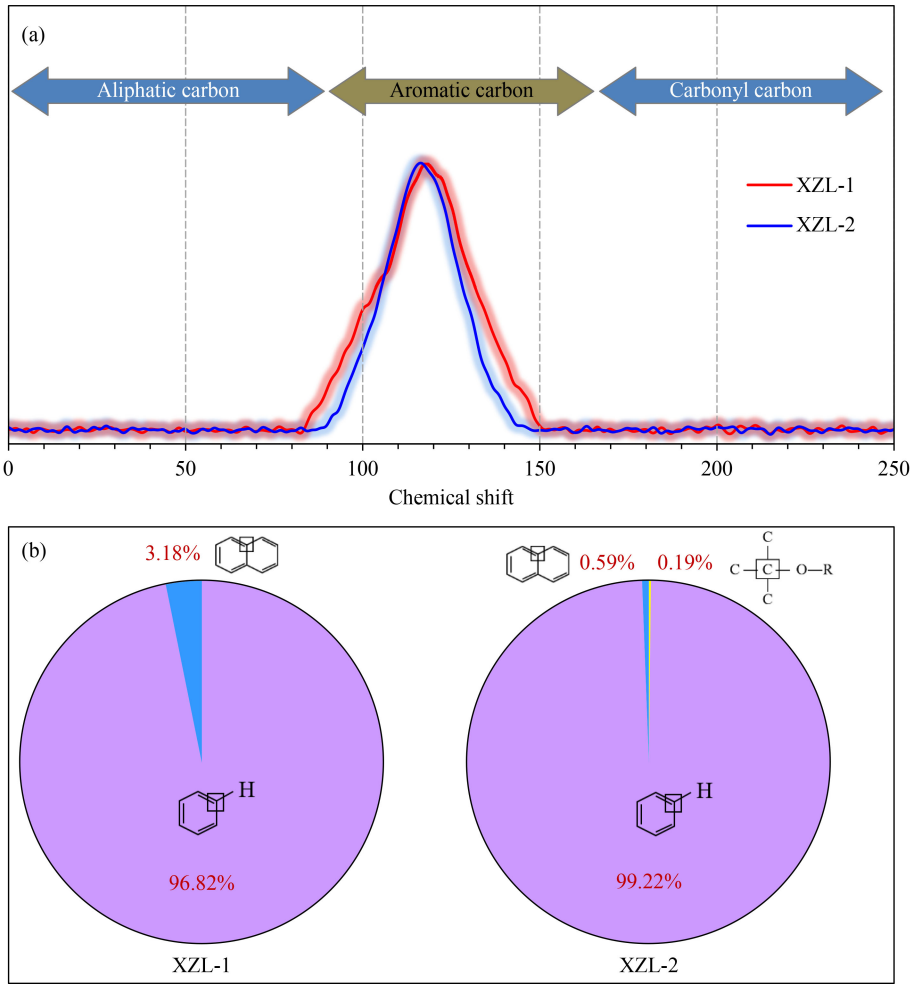

Fig. 4 Chemical structure characteristics of kerogen fractions: (a) ^{13}C-NMR spectra and (b) distribution of organic carbon.

connected to quaternary carbon.

Previous research shows that 1) during the immature stage, kerogen is generated by bacterial action and condensation polymerization because the C-H bonds of aliphatic in kerogen release and aliphatic-intermolecular pores occur; 2) from low-mature to mature stage, asphaltenes, liquid hydrocarbon, and residual kerogen are generated from thermal-depolymerization, and the cracking of asphalt generate liquid hydrocarbon and marginal-oil pores (liquefied pores); 3) during the high to over-mature stage, hydrocarbon transforms into dry gas, and pores (including intermolecular pores in aromatic and gas pores) generated in organic matter because of the release of C-H bonds in kerogen aromatics. The isomerization and demethylation of aromatic compounds during this stage have a good coupling effect on the change of specific surface area of organic matter (Miao et al., 2017; Gao et al., 2018; Wang et al., 2019). Other studies have reported that the aromatic carbon content of organic matter increases and the aliphatic carbon content decreases during thermal evolution, and as a result, aromatic carbon is enriched in over-mature organic matter (Liu et al., 2017; Miao et al., 2017; Craddock et al., 2018; Xiao et al., 2021). Shale sample XZL is in the over-mature stage, with R_o value of 2.70%, and thus the results are consistent with those of previous studies. In addition, our experiments revealed two other phenomena. 1) There is a small difference in the molecular compositions of the organic fractions with different densities in the over-mature marine shale. 2) The organic fractions with different densities underwent different processes during the thermal evolution of the shale.

The higher proportion of aromatic carbon and lack of aliphatic carbon in XZL-1 compared with XZL-2 indicates that the low density organic matter fraction evolved faster than the high density fraction during the thermal evolution. Previous studies on the relationships between the chemical compositions, density, and thermal evolution of the macerals in coal revealed that the hydrocarbon generation potential is in the order of exinite > vitrinite > coal > fusinite during thermal evolution, while both the hydrogen content and density follow the sequence of fusinite > coal > vitrinite > exinite (Chang et al., 2008; Liu et al., 2008; Zhao et al., 2010). Our experimental results suggest that the organic fractions with different densities have different hydrocarbon generation

potentials and underwent a different thermal evolution process, even though these fractions belong to a single maceral (sapropelite). The development of secondary pores is controlled by the hydrocarbon generation potential of the organic matter (Hong et al., 2020; Liu et al., 2022).

3.3 Pore characteristics of different organic fractions

The isotherm N_2 adsorption/desorption curves of the organic fractions are shown in Fig. 5(a). Not all of the curves contain distinct inflection points in the low relative pressure section ($P/P_0 < 0.8$), and the curves increase sharply in the high relative pressure section, which is characteristic of a type III curve according to the International Union of Pure and Applied Chemistry (IUPAC).

The characteristics of the micropores were analyzed via CO_2 isothermal adsorption, and the adsorption curves of the organic fractions are presented in Fig. 5(b). XZL-1 and GZW-1 have much higher CO_2 adsorption capacities than XZL-2 and GZW-2, indicating that the low density organic fraction has a higher CO_2 adsorption capacity than the high density organic fraction.

Based on the N_2 adsorption data, the pore volumes in the diameter range of 1.48–120 nm were calculated. The pore volumes of XZL-1, XZL-2, GZW-1, and GZW-2 are 0.0495 cm^3/g, 0.2537 cm^3/g, 0.0099 cm^3/g, and 0.1180 cm^3/g, respectively, indicating that the high density organic fractions make a larger contribution to the volumes of the mesopores and macropores than the low density organic fractions. The size distribution of the

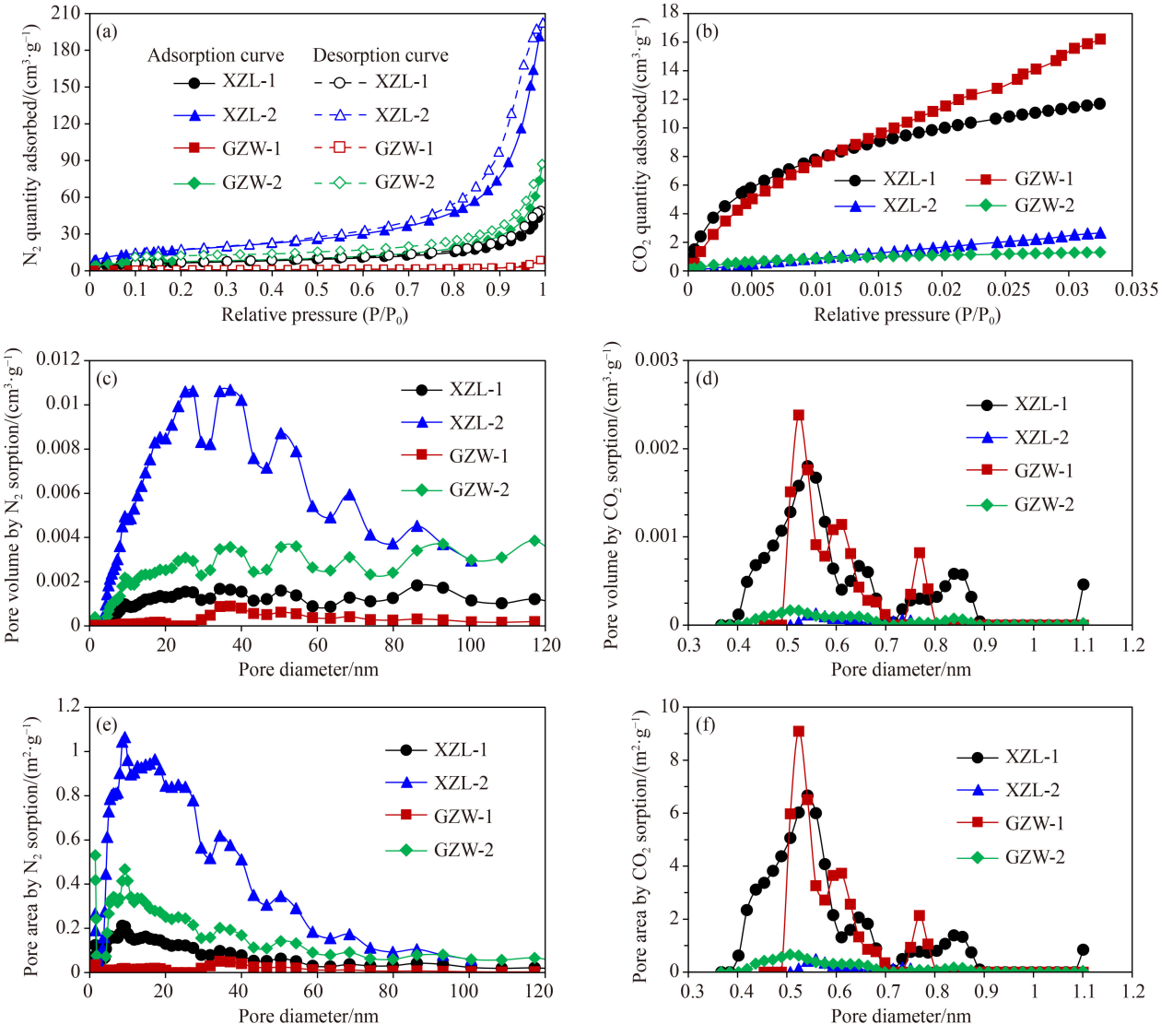

Fig. 5 Isotherm curve and pore size distribution of kerogen fractions: (a) N_2 adsorption/desorption curves; (b) CO_2 adsorption curves; (c) pore volume distribution determined by N_2 adsorption; (d) pore volume distribution determined by CO_2 sorption; (e) pore area distribution determined by N_2 adsortption; (f) pore area distribution determined by CO_2 adsortption.

1.48–120 nm diameter pores (Fig. 5(c)) shows that all of the fractions have multiple peaks, such as at 25 nm, 35 nm, 50 nm, 70 nm, and 90 nm. It should be noted that XZL-2 and GZW-2 have larger pore volumes and surface areas than XZL-1 and GZW-1 in the entire range (Figs. 5(c) and 5(e)). The results imply that the organic fractions with different densities have significantly different pore characteristics, and the high density fraction contains abundant mesopores and macropores.

The pore volume and surface area in the diameter range of 0.36–1.11 nm was calculated from the CO_2 adsorption data. Both the volumes and surface areas of the low density fractions (XZL-1: volume of 0.0185 cm^3/g and surface area of 64.44 m^2/g; GZW-1: 0.0130 cm^3/g and 44.886 m^2/g) are much larger than those of the high density fractions (XZL-2: 0.0009 cm^3/g and 2.87 m^2/g; GZW-2: 0.0019 cm^3/g and 13.36 m^2/g) (Figs. 5(d) and 5(f)). This indicates that the micropores are more enriched in the low density fractions, which is opposite to the distribution of the mesopores and macropores based on the N_2 adsorption data.

Xie et al. (2020) discovered that low density organic fractions which have lots of telalginite and lamalginite macerals (1.06–1.23 g/mL) generated much more light and heavy hydrocarbons than the high density organic fractions which have a lot of detrovitrinite (1.26–1.30 g/mL) in oil shale. Low density organic fractions are characterized by greater amounts of aliphatic compounds, whereas high density organic fractions have larger amounts of aromatic compounds. It is the essence of the evolution of different types of organic matter pores that aromatic carbon rearrangement and aliphatic chains and carbon-heteroatom bond were broken in kerogen. Kerogen transforms from a disordered structure to a graphite crystal structure in the course of thermal evolution. The condensation reaction leads to the closing of organic matter pores. In recent years, through thermal maturity experiments, many scholars have found when thermal maturity is in the high to over-mature stage, kerogen and pyrobitumen had more micropores, and the porosity of organic matter were decreased. (Liu et al., 2013; Wang et al., 2016a; Tenger et al., 2021; Xu et al., 2021; Xu et al., 2022a; Xu et al., 2022b). Based on the above, the low density organic matter fractions (XZL-1 and GZW-1) have more micropores and the high density fractions (XZL-2 and GZW-2) have more mesopores and macropores, which shows the evolution degree of the low density fractions is higher than that of the high density fractions.

3.4 Implication in reservoir evaluation of over-mature marine shale

The above discussion demonstrates that the organic fractions with various densities in the over-mature marine shale have significantly different pore characteristics and molecular compositions. Thus, it is important to determine whether these organic fractions have markedly different occurrence states.

In this study, sample XZL is argillaceous shale with a clay mineral content of 59.20% (Table 1). In this sample, most of the organic matter is combined with clay minerals to form organo-clay composites (Figs. 6 and 9(b)), and the remaining organic matter is distributed in the intergranular pores and fractures or is dispersed in the matrix. The weight ratio between XZL-2 and XZL-1 is about 1.68:1, indicating that about two-fifths of the organic matter in sample XZL has a density of less than 1.25 g/cm^3.

Sample GZW is a siliceous shale with a quartz content of 58.60%, and most of the organic matter in this sample is distributed in the intergranular pores between the quartz particles (Figs. 6 and 9(b)). The proportion of the high density organic fraction is 81.75%, and only a small part of the organic matter has a density of less than 1.25 g/cm^3.

Ye et al. (2009) and Fan et al. (2010) used the separation of organic matter components and fluorescence analysis to discover the relationship between organic matter density and organic matter. It is difficult to use fluorescence analysis to distinguish organic matter in the over-mature marine shale. Scanning electron microscopy is the most effective way to identify organic matter; recent studies have found that the organic pore structures of the different occurrence states of organic matter are significantly different. The main differences are 1) pyrobitumen is much more porous than solid kerogen (Hong et al., 2020; Wang et al., 2020; Zhang et al., 2020); 2) amorphous pyrobitumen is rich in mesopores, while spherical pyrobitumen is mainly rich in macropores (Zhang et al., 2020; Xie et al., 2021); 3) in over-mature marine shale, organic matter is weak in fluorescence and solubility, making it difficult to accurately distinguish the types of microscopic components. So Zhang et al. (2017, 2019) divided the organic matter in the Niutitang over-mature marine shale into four types according to their occurrence states (they are banded, massive, filled, and mutually wrapped organic matter); and 4) organic matter pores are better preserved in siliceous shale than in argillaceous shale because siliceous shale has a rigid skeleton composed of quartz particles (Wang et al., 2016b; Dong et al., 2021; Gao et al., 2021; Xie et al., 2021). These phenomena can also be observed in Fig. 6. Although the experiments conducted in this study cannot directly reflect the relationship between the occurrence state and density of organic matter, it is obvious that the organic pore structure is closely related to both the occurrence state and the density of the organic matter.

The scanning electron microscope images acquired in this study show that the banded and filled organic matter do not contain pores, while the massive and mutually wrapped organic matter is rich in pores (Fig. 6). From the qualitative evaluation of scanning electron microscope

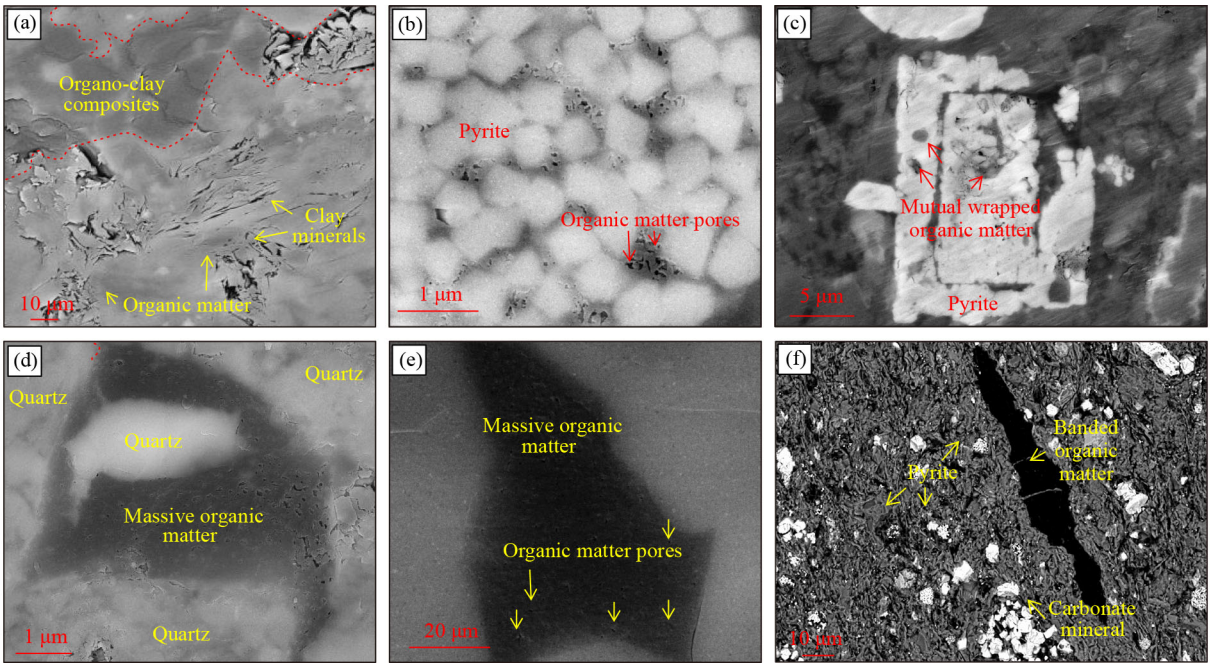

Fig. 6 Scanning electron microscope images of XZL (a, b, c) and GZW (d, e, f) shale samples.

images, it can be seen that the mutually wrapped organic matter develops mesopores and macropores (Figs. 6(b) and 6(c)). The massive organic matter usually develops micropores and mesopores (Figs. 6(d) and 6(e)). We also found that different types of pores developed in different organic matter components in the Niutitang samples from other regions (Fig. 7). The development of organic matter pores are consistent with Fig. 6. According to EDS analysis (Fig. 8), the C/O of organic matter in different occurrence states are obviously different, which proves that the types of organic matter are different and density of the organic fraction are different. The organic matter pores developed by different occurrence states of organic matter are of different sizes, which is almost consistent with the pore relationship of organic components with different density, but we need more evidence to prove it.

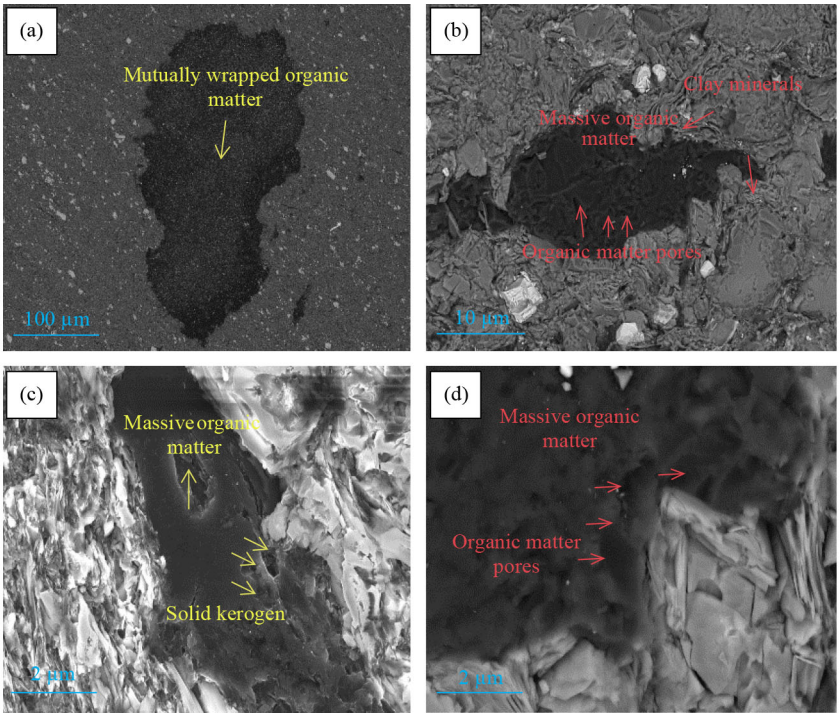

Fig. 7 Scanning electron microscope images of ZK-4 shale samples from Songtao County.

In contrast to shale sample GZW, which is rich in quartz, shale sample XZL has a much higher clay mineral content (Table 1). In shale sample XZL, most of the organic matter is mutually wrapped with clay minerals, while most of the organic matter is massive in shale sample GZW and is surrounded by quartz, indicating that the main occurrence states of the organic matter in these shales are different. In addition, shale sample GZW has a much higher proportion of low density organic matter than shale sample XZL (Fig. 9(a)). Does this imply that the densities of the organic matter in the intergranular pores and the organic matter combined with the clay minerals are different? This is an interesting phenomenon, and it will provide new methods for reservoir evaluation of over-mature marine shale if the real relationships between the density, occurrence, and pore structure can be determined.

4 Conclusions

1) Aromatic carbon is the dominant molecular composition of the over-mature organic matter in the Lower Cambrian Niutitang shale. During the over-mature stage, the organic fractions with densities of greater than and

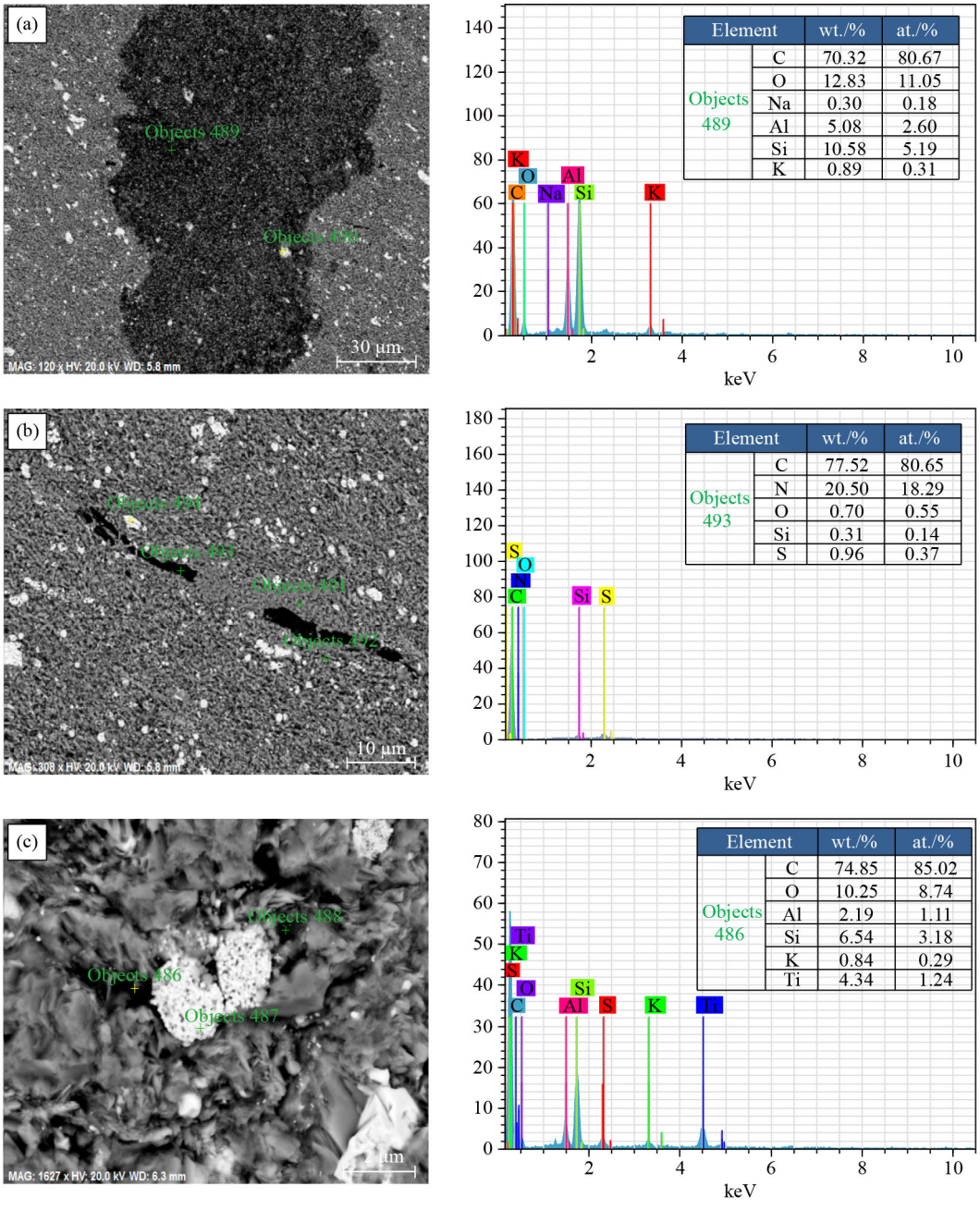

Fig. 8 SEM pictures and EDS analysis of ZK-4 shale samples.

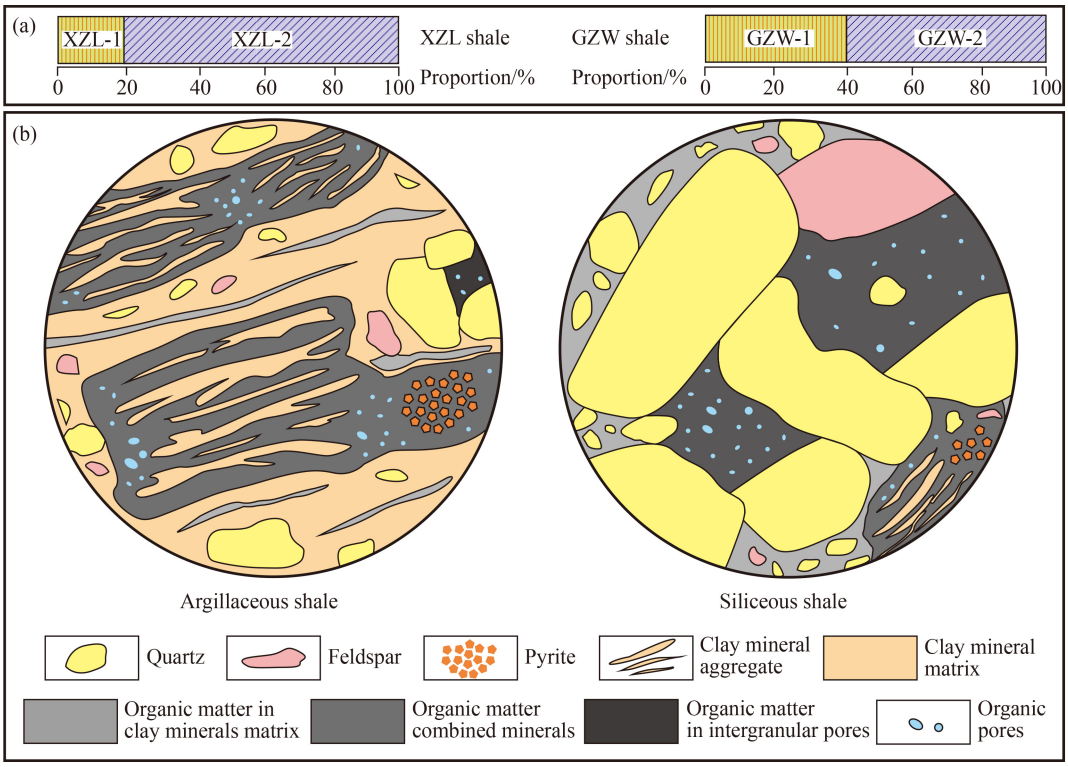

Fig. 9 (a) Proportions of organic fractions in XZL and GZW shale samples. (b) Schematic diagram for compositions in argillaceous and siliceous shales from the Lower Cambrian Niutitang formation.

less than 1.25 g/cm^3 do not have significantly different molecular compositions.

2) The organic fractions with densities of greater than and less than 1.25 g/cm^3 have significantly different organic matter pore characteristics. In contrast to the high density organic fraction, the low density fraction contains abundant micropores and lacks mesopores and macropores.

3) The organic pore structures of the organic matter with different occurrence states are significantly different. The organic pore structure is closely related to both the occurrence state and density of the organic matter. However, this relationship is still unclear and requires further study.

Acknowledgments This work was financially supported by the National Natural Science Foundation of China (Grant Nos. 42002166 and 42162016) and the Guizhou Provincial Fund Project (Nos. [2020]1Y161 and ZK[2022]106).

References

Chang H, Zeng F, Li W, Li M, Li J, Xie K (2008). Semicoke contraction kinetics of coal and its macerals in pyrolysis. Acta Physico-Chimica Sinica, 24(4): 675–680

Chen D, Wang J, Qing H, Yan D, Li R (2009). Hydrothermal venting activities in the Early Cambrian, south China: petrological, geochronological and stable isotopic constraints. Chem Geol, 258(3–4): 168–181

Chen L, Jiang Z, Liu K, Tan J, Gao F, Wang P (2017). Pore structure characterization for organic-rich Lower Silurian shale in the Upper Yangtze Platform, south China: a possible mechanism for pore development. J Nat Gas Sci Eng, 46: 1–15

Clarkson C R, Freeman M, He L, Agamalian M, Melnichenko Y B, Mastalerz M, Bustin R M, Radliński A P, Blach T P (2012). Characterization of tight gas reservoir pore structure using USANS/SANS and gas adsorption analysis. Fuel, 95: 371–385

Craddock P R, Bake K D, Pomerantz A E (2018). Chemical, molecular, and microstructural evolution of kerogen during thermal maturation: case study from the woodford shale of Oklahoma. Energy Fuels, 32(4): 4859–4872

Dong T, He Q, He S, Zhai G, Zhang Y, Wei S, Wei C, Hou Y, Guo X (2021). Quartz types, origins and organic matter-hosted pore systems in the lower cambrian Niutitang Formation, middle yangtze platform, China. Mar Pet Geol, 123: 104739

Dyrkacz G R, Bloomquist C, Ruscic L (1984). High-resolution density variations of coal macerals. Fuel, 63(10): 1367–1373

Fan F, Cai J, Song M, Bao Y (2010). An exploratory study on density fractionation and organic matter preservation of muddy source rock. J Tongji U (Nat Sci), 39(9): 1359–1364 (in Chinese)

Feng Z, Hao F, Zhou S, Wu W, Tian J, Xie C, Cai Y (2020). Pore characteristics and methane adsorption capacity of different lithofacies of the Wufeng Formation–Longmaxi Formation shales, southern Sichuan Basin. Energy Fuels, 34(7): 8046–8062

Gao Y, Zou Y, Liang T, Peng P (2017). Jump in the structure of Type I kerogen revealed from pyrolysis and 13CDP MAS NMR. Org Geochem, 112: 105–118

Gao Z, Liang Z, Hu Q, Jiang Z, Xuan Q (2021). A new and integrated imaging and compositional method to investigate the contributions of organic matter and inorganic minerals to the pore spaces of lacustrine shale in China. Mar Pet Geol, 127(6): 104962

Gao Z, Yang S, Jiang Z, Zhang K, Chen L (2018). Investigating the spontaneous imbibition characteristics of continental Jurassic Ziliujing Formation shale from the northeastern Sichuan Basin and correlations to pore structure and composition. Mar Pet Geol, 98: 697–705

GB/T 19144–2010 (2010). Isolation method for kerogen from sedimentary rock. Standardization Administration of the People's Republic of China: 1–7

Guo Y, Tang Y, Wang S, Li W, Jia L (2013). Maceral separation of bark liptobiolite and molecular structure study through high resolution TEM images. China Coal Soc, 38(6): 1019–1024

Han H, Cao Y, Chen S, Lu J, Huang C, Zhu H, Zhan P, Gao Y (2016). Influence of particle size on gas-adsorption experiments of shales: an example from a Longmaxi Shale sample from the Sichuan Basin, China. Fuel, 186: 750–757

Hong J, Tang X, Zhang C, Huang H, Shan Y, Zheng Y, Xie H (2020). Characteristics and controlling factors of organic-matter pores in Longmaxi Formation shale, middle Yangtze Region: a case study of Well YY3. Oil Gas Geol, 41(5): 1060–1072

Hu T, Pang X, Jiang S, Wang Q, Zheng X, Ding X, Zhao Y, Zhu C, Li H (2018). Oil content evaluation of lacustrine organic-rich shale with strong heterogeneity: a case study of the Middle Permian Lucaogou Formation in Jimusaer Sag, Junggar Basin, NW China. Fuel, 221: 196–205

Ji W, Hao F, Schulz H M, Song Y, Tian J (2019). The architecture of organic matter and its pores in highly mature gas shales of the lower Silurian Longmaxi Formation in the upper Yangtze platform, south China. AAPG Bull, 103(12): 2909–2942

Joyner L G, Barrett E P, Skold R (1951). The determination of pore volume and area distributions in porous substances. II. Comparison between nitrogen isotherm and mercury porosimeter methods. J Am Chem Soc, 73(7): 3155–3158

Klimakow M, Klobes P, Rademann K, Emmerling F (2012). Characterization of mechanochemically synthesized MOFs. Microporous Mesoporous Mater, 154: 113–118

Liu B, Mastalerz M, Schieber J (2022). SEM petrography of dispersed organic matter in black shales: a review. Earth Sci Rev, 224: 103874

Liu D, Xiao X, Tian H, Min Y, Zhou Q, Cheng P, Shen J G (2013). Sample maturation calculated using Raman spectroscopic parameters for solid organics: methodology and geological applications. Chin Sci Bull, 58(11): 1285–1298

Liu Q, Bernhard M, Jin Z, Wang Y, Jan H, Ralf L, Liu W (2008). Comparison of the gas compound generation of tarim coal and its macerals in open system non-isothermal pyrolysis with ultra-high temperature. Nat Gas Geosci, 19(6): 748–753

Liu X, Luo D, Xiong J, Liang L (2017). Construction of the average molecular modeling of the kerogen from the Longmaxi formation. Chemical Ind Eng Progress, 36(2): 530–537 (in Chinese)

Liu Y, Liu S, Zhang R, Zhang Y (2021). The molecular model of Marcellus shale kerogen: experimental characterization and structure reconstruction. Int J Coal Geol, 246: 103833

Loucks R G, Reed R M, Ruppel S C, Hammes U (2012). Spectrum of pore types and networks in mudrocks and a descriptive classification for matrix-related mudrock pores. AAPG Bull, 96(6): 1071–1098

Miao Y, Li X, Wang X, Chen Y, Zhou Y, Liu F, Xia J (2017). Review on hydrocarbon generation, pores formation and its methane adsorption mechanism in shale kerogen. Sci China Phys Mech Astron, 47(11): 41–51

Milliken K L, Rudnicki M, Awwiller D N, Zhang T (2013). Organic matter–hosted pore system, Marcellus Formation (Devonian), Pennsylvania. AAPG Bull, 97(2): 177–200

Ning S, Xia P, Hao F, Tian J, Zhong Y, Zou N, Fu Y (2021). Shale facies and its relationship with sedimentary environment and organic matter of Niutitang black shale,Guizhou Province. Nat Gas Geosci, 32(9): 1297–1307

Okolo G N, Everson R C, Neomagus H W J P, Roberts M J, Sakurovs R (2015). Comparing the porosity and surface areas of coal as measured by gas adsorption, mercury intrusion and SAXS techniques. Fuel, 141: 293–304

Slatt R M, O'Brien N R (2011). Pore types in the Barnett and Woodford gas shales: contribution to understanding gas storage and migration pathways in fine-grained rocks. AAPG Bull, 95(12): 2017–2030

Tenger B, Lu L, Yu L, Zhang W, Pan A, Shen B, Wang Y, Yang Y, Gao Z (2021). Formation, preservation and connectivity control of organic pores in shale. Pet Explor Dev, 48(4): 687–699

Wang B, Wang C, Wang X, Peng Z, Wei K (2019). Characteristics of aromatic compounds in high-over matured marine shale and its significance to shale gas. Earth Sci, 44(11): 3705–3716

Wang P, Zhang C, Li X, Zhang K, Yuan Y, Zang X, Cui W, Liu S, Jiang Z (2020). Organic matter pores structure and evolution in shales based on the he ion microscopy (HIM): a case study from the Triassic Yanchang, Lower Silurian Longmaxi and Lower Cambrian Niutitang shales in China. J Nat Gas Sci Eng, 84: 103682

Wang Q, Yao C, Zhou Y, Che Y, Liu H, Zhao X, Zhang Y (2022b). The relationship between the oil shale density and the structural features of corresponding kerogens. Carbon Resources Conversion, 5(1): 84–91

Wang R, Ding W, Zhang Y, Wang Z, Wang X, He J, Zeng W, Dai P (2016b). Analysis of developmental characteristics and dominant factors of fractures in Lower Cambrian marine shale reservoirs: a case study of Niutitang formation in Cen'gong block, southern China. J Petrol Sci Eng, 138: 31–49

Wang R, Gu Y, Ding W, Gong D, Yin S, Wang X, Zhou X, Li A, Xiao Z, Cui Z (2016a). Characteristics and dominant controlling factors of organic-rich marine shales with high thermal maturity: a case study of the Lower Cambrian Niutitang Formation in the Cen'gong block, southern China. J Nat Gas Sci Eng, 33: 81–96

Wang R, Hu Z, Long S, Du W, Wu J, Wu Z, Nie H, Wang P, Sun C, Zhao J (2022a). Reservoir characteristics and evolution mechanisms of the Upper Ordovician Wufeng-Lower Silurian Longmaxi shale, Sichuan Basin. Oil Gas Geol, 43(2): 353–364

Wang T C, Bury W, Gómez-Gualdrón D A, Vermeulen N A, Mondloch J E, Deria P, Zhang K, Moghadam P Z, Sarjeant A A,

Snurr R Q, Stoddart J F, Hupp J T, Farha O K (2015). Ultrahigh surface area zirconium MOFs and insights into the applicability of the BET theory. J Am Chem Soc, 137(10): 3585–3591

Wang Y, Liu L, Cheng H (2021). Gas adsorption characterization of pore structure of organic-rich shale: insights into contribution of organic matter to shale pore network. Nat Resour Res, 30(3): 2377–2395

Xia P, Fu Y, Yang Z, Guo C, Huang J, Huang M (2020). The relationship between sedimentary environment and organic matter accumulation in the Niutitang black shale in Zhenyuan, northern Guizhou. Acta Geol Sin, 94(3): 947–956

Xia P, Li H, Fu Y, Qiao W, Guo C, Yang Z, Huang J, Mou Y (2021). Effect of lithofacies on pore structure of the Cambrian organic-rich shale in northern Guizhou, China. Geol J, 56(2): 1130–1142

Xiao W, Cao J, Liao Z, Hu G, Zuo Z, Hu K (2021). Elemental geochemistry proxies recover original hydrogen index values and total organic carbon contents of over-mature shales: Lower Cambrian south China. Chem Geol, 562: 120049

Xie G, Liu S, Jiao K, Deng B, Ye Y, Sun W, Li Z, Liu W, Luo C, Li Z (2021). Organic pores in deep shale controlled by macerals: classification and pore characteristics of organic matter components in Wufeng Formation-Longmaxi Formation of the Sichuan Basin. Nat Gas Ind, 41(9): 23–34

Xie X, Li M, Xu J, Snowdon L, Volkman J (2020). Geochemical characterization and artificial thermal maturation of kerogen density fractions from the Eocene Huadian oil shale, NE China. Org Geochem, 144: 103947

Xu J, Zhang C, Xi X, Rui X (2018). Separation of macerals in organic-rich source rocks and their geochemical characteristics. Petroleum Geology & Experiment, 40(6): 828–835

Xu L, Yang K, Lu W, Li X, Wei H (2022a). New research progress on organic-rich shale micro- and nanoscale pore system evolution characteristics and models. Acta Sediment Sin, 40(1): 1–21

Xu L, Yang K, Zhang L, Liu L, Jiang Z, Li X (2021). Organic-induced nanoscale pore structure and adsorption capacity variability during artificial thermal maturation: pyrolysis study of the Mesoproterozoic Xiamaling marine shale from Zhangjiakou, Hebei, China. J Petrol Sci Eng, 202: 108502

Xu L, Yang W, Jiang Z, Chen D, Wang Y, Lu J, Zhao M, Li L (2022b). Evolution and genesis of organic pores in Triassic Xujiahe Formation shale, Western Sichuan Depression, Sichuan Basin. Oil Gas Geol, 43(2): 325–340

Yan Y, Qi Y, Marshall M, Jackson W R, Chaffee A L (2019). Separation and analysis of maceral concentrates from Victorian brown coal. Fuel, 242: 232–242

Ye W, Cai J, Fan F, Bao Y, Xe J (2009). Argillaceous hydrocarbon source rock density separation and distribution of organic carbon. Geo J China U, 15(4): 547–556

Yuan Y, Rezaee R, Yu H, Zou J, Liu K, Zhang Y (2021). Compositional controls on nanopore structure in different shale lithofacies: a comparison with pure clays and isolated kerogens. Fuel, 303: 121079

Zhang H, Jiao S, Lin B, Hao L, Yuan L (2017). Genetic relationship between organic matters and minerals in the Lower Cambrian shale in Yangze Plate. Nat Gas Explor Develop, 40(4): 25–33 (in Chinese)

Zhang H, Yuan L, Zhang Y, Jiao S, Lin B, Yang Q (2019). Microcosmic biomarker of organic matter in sweet spots from marine shale gas. Nat Gas Explor Develop, 42(3): 38–45 (in Chinese)

Zhang W, Hu W, Borjigin T, Zhu F (2020). Pore characteristics of different organic matter in black shale: a case study of the Wufeng-Longmaxi Formation in the southeast Sichuan Basin, China. Mar Pet Geol, 111: 33–43

Zhao Y, Hu H, Jin L, He X, Zhu S (2010). Pyrolysis behavior of macerals from weakly reductive coals. Energy Fuels, 24(12): 6314–6320